Bestimmung der Schließung und Öffnung von Mikrospalten mit auf verschiedenen Belastungswegen ausgeführten triaxialen Versuchen

Determining the Microcracks Closure and Opening with Different Loading Paths Triaxial Tests

Teach. Ass. Vásárhelyi, Balázs – *Technical University of Budapest, Budapest, Hungary*
Ass. Prof. Deli, Árpád – *Technical University of Budapest, Budapest, Hungary*

ABSTRACT: *This paper discusses a complex investigation to determine the microcrack closure and opening, with four different triaxial tests of a homogeneous isotropic limestone. Two of the researches were under drained conditions (deviatoric triaxial test and triaxial test with constantly increasing stress) and two of them were under undrained conditions (triaxial test connected with decreasing confining pressure and triaxial test with constantly increasing stress). During the tests the uniaxial and the confining pressure, the pore-fluid pressure, and the axial and the lateral strains were measured continuously.*

ZUSAMMENGFASSUNG: *In diesem Artikel wird eine komplexe Experimentenserie zur Bestimnung der Schliessung und Öffnung von Mikrospalten dargestellt, die aus vier verschiedenent auf homogenem isotropem Kalkstein ausgeführten triaxialen Untersauchungen besteht. Zwei von diesen Experimenten waren drainiert (erstens eine deviatorisch-triaxiale Unterschuchung, zweitens eine triaxiale Untersuchung mit ständig wachsender Spannung), undzwei waren undrainiert (eine triaxiale Untersuchung in Bezug auf abnehmenden Seitendruck und eine triaxiale Untersuchung mit ständig wachsender Spannung). Während der Experimenten wurden der uniaxiale und der Seitendruck, der Porenflüssigkeitsdruck und die axialen und lateralen Deformationen stets gemessen.*

1. Introduction

The failure process of brittle rock has been investigated by several researchers (e.g.: 1-7, etc.) with uniaxial compression tests. Using the stress-strain diagrams, the stages of crack developments and measuring the axial and lateral strains the crack volume strains can be calculated (6).

Between the crack closure and the yield stress, the axial stress-strain curve behaves elastically and its slope (the axial stiffness) should define the elastic modulus (E). Elastic conditions prevail at low stress, before the crack initiation point. Cook (8) proved that the volumetric strain of a sample measured by surface strain gauges was a pervasive volumetric property of the rock and not a superficial phenomenon. For a cylindrical sample subjected to axial loading, with or without a confining stress, and under small strains, the volumetric strain from the axial strain (e_a) and the lateral strain (e_l) curve is given by

$$e_v = \frac{\Delta V}{V} \cong 2\, e_l + e_a \qquad (1)$$

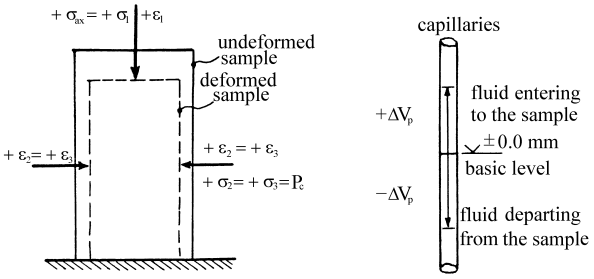

Fig. 1. Convention of the signs.

The pore volumetric strain is the excess of the measured entered or departed fluid (ΔV_P) (the conventions according to Fig. 1) divided by the pore volume (V_P) which is reached by the fluid during the saturation:

$$\Theta = \frac{\Delta V_P}{V_P} \qquad (2)$$

If the saturation of the rock is perfect, thus there are not closed pore in the sample, the changing of the pore volumetric strain is in ratio of the crack volumetric strain.

The goal of this paper is to present a complex investigation to determine the microcrack closure and opening with four different triaxial tests. The examined limestone was saturated and the different tests were carried out under drained and undrained conditions. The fracture process has been investigated using the same triaxial tests with saturated sandstone (9, 10).

2. Material Description, Specimen Preparation and Test Equipment

A homogeneous, isotropic Jurassic limestone (from Lavoux, France) was examined. Table 1 and 2 show the measured petrophysical constants and the minerals with their volume percentage, respectively. There are not pores inside the minerals.

The diameter and the length of each cylindrical test specimen was 38 mm and 76 mm long, respectively and each sample was dried during 72 hours in 60 °C before they were equipped with two axial and two lateral strain gauges that were attached to the middle third of the specimen to avoid end effects. Recording the axial (e_a) and lateral (e_l) strains in a sample as it is loaded with or without confining stress was carried out according to the standard (11).

Petrophysical constants	**Unit**	**Result**
Density (dried), r_d	kg/m^3	2119
Density (saturated), r_w	kg/m^3	2334
Grain density, r_s	kg/m^3	2700
Apparent porosity, n_w	%	21.28
Total porosity, n_t	%	21.51
Secondary micro-pore porosity, n_{w0}	%	-
Micro-cracks closing pressure, P_f	MPa	-

Table 1: Measured pertophysical constant of the examined limestone.

Petrographic constituents	**V %**	**Grain size (mm)**		
		Min.	Aver.	max.
Microoncoids	39.0	0.025	0.27	0.65
Bioclastics	32.0	0.05	0.55	0.20
Cement (micrit)	26.5	0.001	0.005	0.10
Limonite	0.5	-	-	-
Porosity	2.5	< 0.005	0.075	0.37

Table 2: Petrographic constituents of the investigated rock

.

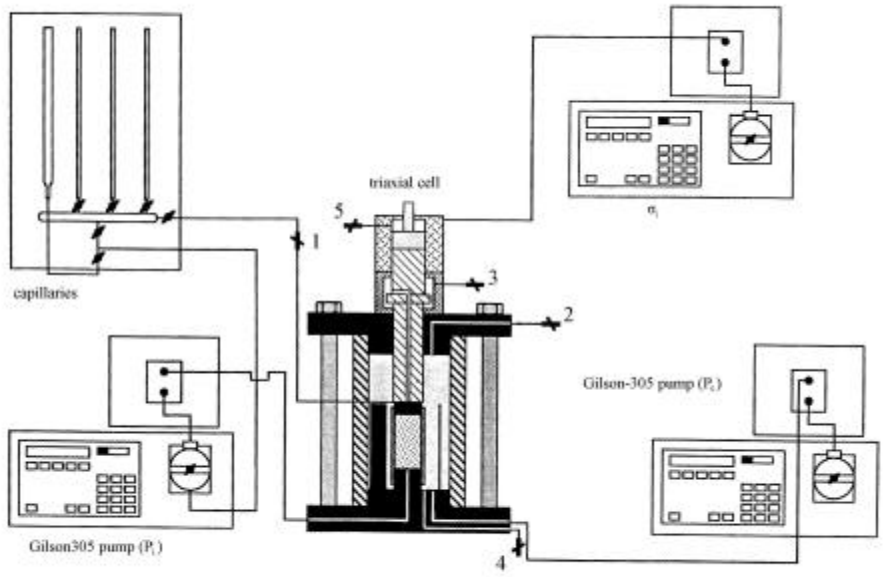

Fig. 2: Schematic diagram of the test arrangement. Tap 1: open position: drained / closed position: undrained condition. Taps 2-5: for oil and air regulate.

The saturation was carried out after the drying: firstly the specimens were saturated with water for 24 hours in a glass vessel with thin air, afterwards the samples were in water for 48 hours long under atmospheric pressure. Finally all the samples were covered with a rubber jacket to protect them from the oil during the triaxial tests.

Fig. 2 shows schematically the arrangement of the test equipment. The capacity of the triaxial cell was 100 MPa and it was connected with two Gilson-305 type pumps (capacity: 60 MPa) which were used to regulate both the confining pressure (P_c) and the injection for the pore-fluid pressure. The measurement sensitivity of both the pore water-pressure and the confining pressure (P_c) was 0.01 MPa. Capillaries with different diameters were used to determine the volume of the pore water. The deformation was measured with two LVTD.

At room-temperature (22 °C) the samples were saturated with methanol. Therefore the pore water pressure (P_i = 1 MPa) chosen was lower than the starting point of the hydrostatic pressure ($s_1 = s_3 = P_c$ = 2 MPa) in the Gilson-pump used for producing the required pore fluid pressure (Fig. 2) and the tap for draining was open thus the air of the pores was mixing with the methanol and getting out across the tap. After 15-17 hours the saturation was complete.

Since quasi-static loading rates were intended to make thus the strain rate ($\dot{e}$) was 10^{-6}/sec in case of undrained deviatoric triaxial tests and the constant stress rate ($\dot{s}$) was 5×10^{-3} MPa/sec in case of the other investigations.

3. Applied Loading Paths

The researches were carried out with the following triaxial tests:

a) drained condition: deviatoric triaxial test and triaxial test with constantly increasing stress;
b) undrained condition: triaxial test connected with decreasing confining pressure and triaxial test with constantly increasing stress.

3.1 Undrained, Deviatoric Triaxial Test

Fig. 3 shows the applied stress path, where

0: hydrostatic starting point, where $P_c = s_1^0 = 2$ MPa;

0A: drained hydrostatic loading till $P_c = s_1 = 30$ MPa ($\dot{e} = 10^{-6}$/sec). During this period tap 1 was open, i.e. $P_i = 0$ MPa;

A: Setting the starting value of the pore fluid pressure (P_i^0 = 1 MPa). Tap 1 was closed. Starting from point A P_c was constant (30 MPa) and deviatoric stress was applied under undrained condition ($\dot{e} = 10^{-6}$/sec).

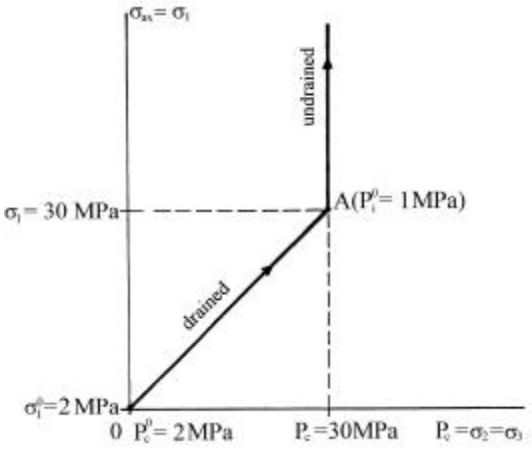

Fig. 3: Loading path of the undrained deviatoric triaxial test ($\dot{e}_{ax}$ =10^{-6}/sec)

3.2 Undrained Triaxial Test with Constantly Increasing Stress

The applied stress path can be seen in Fig. 4. In case of the undrained test tap 1 was closed.

0: Hydrostatic starting point ($P_c^0 = s_1^0 = 1$ MPa) and setting the starting value of the pore fluid pressure (P_i^0 =1 MPa);

0-A-B…: Applying Δs_1 and Δs_3 axial and lateral stresses with increasing rate with k = 10 and k = 20 values ($k = \Delta s_1 / \Delta s_3$). The loading rate ($\dot{s}^1$) was 5×10^{-3} MPa/sec and Δs_3 = 0.1 MPa.

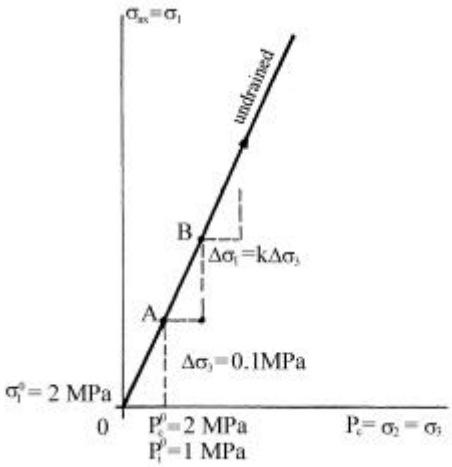

Fig. 4: Applied loading path for undrained, constant stress increasing triaxial test ($\dot{s}_{ax}$ =5×10^{-3} MPa/sec)

3.3 Drained Triaxial Test, Connected with Decreasing Confining Pressure

Fig. 5 presents the applied loading path. Tap 1 was open (drained test).

0: hydrostatic starting point with $P_c = s_1^0 = 2$ MPa;

0A: drained hydrostatic loading;

Starting at A: drained unloading in the lateral direction; decreasing the confining stress (P_c) manually with tap 3. The axial stress (s_1) was constant: 60 MPa.

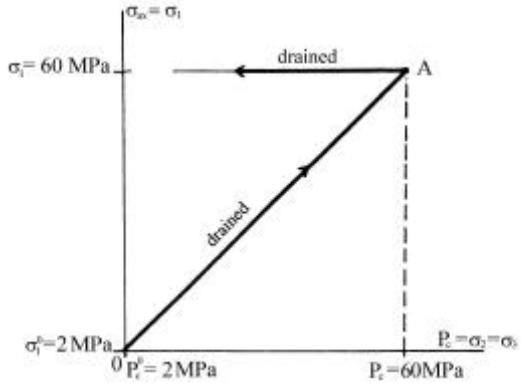

Fig. 5: Applied loading path of drained triaxial test connected with decreasing confining pressure ($\dot{s}$ =5×10^{-3} MPa/sec)

3.4 Drained Triaxial Test with Constantly Increasing Stress

The test was carried out according to the loading path presented in Fig. 6. During the test tap 1 was open (drained test).

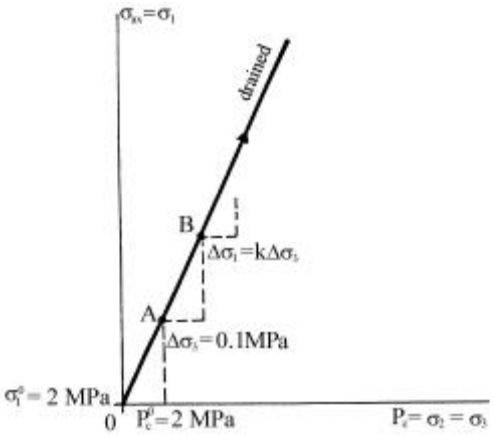

Fig. 6: Loading path of drained triaxial test with constantly increasing stress
($\dot{s}_{ax}$ = 5×10^{-3} MPa/sec).

0: hydrostatic starting point with $P_c = s_1^0 = 1$ MPa;

0-A-B…: Applying Δs_1 and Δs_3 axial and lateral stresses with increasing rates k = 10 and k = 20 values ($k = \Delta s_1 / \Delta s_3$). The loading ($\dot{s}^1$) rate is 5×10^{-3} MPa/sec and Δs_3 = 0.1 MPa.

4. Results and Discussion

4.1 Results of Undrained, Deviatoric Triaxial Test (P_c = 30 MPa)

The deviatoric stress (s_{dev}) in the function of the strains (e_1, e_3, e_v) is shown in Fig. 7. Due to the plastic behaviour of the rock the measurable maximal deviatoric stress in case of e_3 is higher than e_1 or e_v. The non-linearity of the curve is starting at low stress level.

According to Fig. 8, there is an "S-pattern" between the microcrack threshold and the pore-fluid pressure changing (9). Determining the maximum value of P_i from Fig. 8 the stresses are the same level as the microcrack opening limit in Fig. 7. Since the microcracks are opened after this point the pore fluid pressure decreases due to the increasing pore volume. This deviatoric stress is approximately half (54 %) of the failure stress.

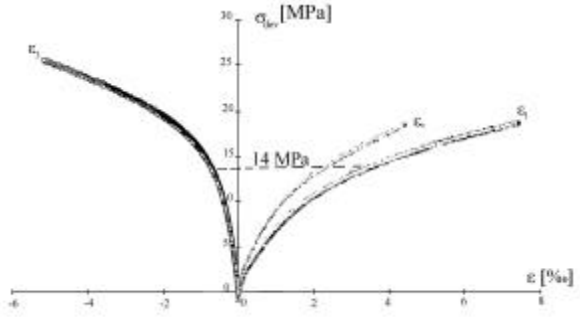

Fig. 7: Deviatoric stress versus strains in case of undrained triaxial test (P_c = 30 MPa).

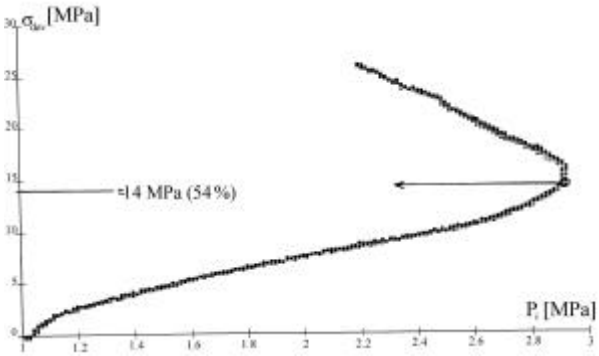

Fig. 8: The relation between the deviatoric pressure and the pore fluid pressure in case of undrained deviatoric test – the "S-pattern" (P_c = 30 MP).

4.2 Results of the Undrained Triaxial Test with Constantly Increasing Stress (k = 10 and k = 20)

The characteristic of the curves are the same as in Figs. 7-8. There are not closing parts of the s_1–e_v curves thus the porosity from the microcracks are neglectable. The maximum of the pore fluid pressure is also at the dilation limit. Because of the increasing volume of the micro-crack system the pore fluid pressure is decreasing after the maximal stress. The strength and the pore fluid pressure are higher if k is smaller. The failure stress is among 75-80 % of the s_3 for the maximal pore fluid pressure and no depend on k.

4.3 Results of the Drained Triaxial Test, Connected with Decreasing Confining Pressure

Till P_c = 20-22 MPa the Q is zero or negative, i.e. fluid entering the sample, thus the microcracks developed during the hydrostatic stress and strain (see Fig. 9).

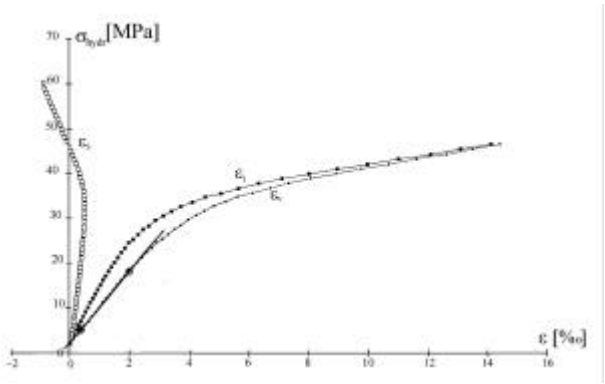

Fig. 9: Changing of the relative pore volume in drained hydrostatic pressure and after lateral load decreasing.

Analysing the s_{hydr}-e curves (Fig. 10) after the linear part till 30-35 MPa e_3 starting decreasing (i.e. the diameter of the sample considering e_3 increases, although the volume of the sample decreases). It means that during the linear part the pore system and the bond among the minerals do not change significantly. During the second part of the curve (after 30-35 MPa) the damage of the pore system is more and more significant.

Fig. 11 presents a measured hydrostatic stress – relative pore volume changing (s_{hydr}-Q) curve. Due to hydrostatic pressure the pore volume, which indicated the small value of the Q at the first part, decreases.

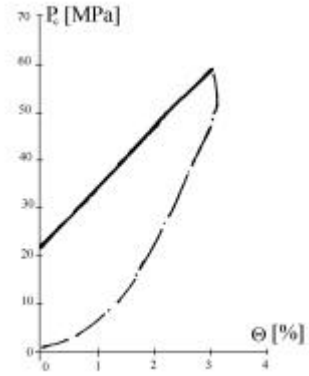

Fig. 10: Drained hydrostatic pressure versus strains.

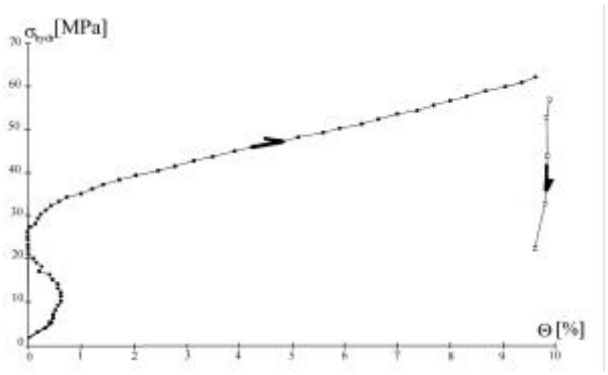

Fig. 11: Confining pressure versus strains for drained triaxial tests with decreasing lateral load.

4.4 Results of the Drained Triaxial Test with Constantly Increasing Stress (k = 10 and 20)

Figs. 12-13 present the measured stress versus strain and relative pore volume change versus pressure curves, respectively, in case of k = 20. The stress of microcracks opening decreases with increasing k (from 40 % to 30 %) but the pattern of the curves are same.

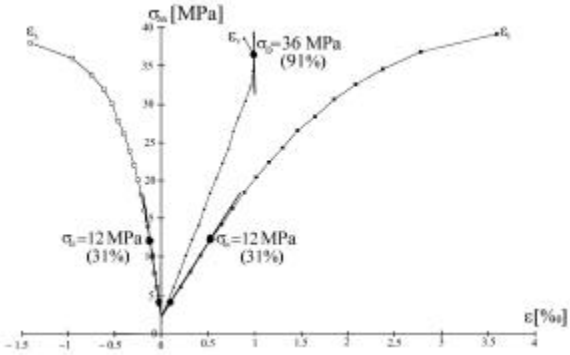

Fig. 12: Stress-strains diagram for the drained triaxial test in case of constantly increasing axial stress (k = 20).

According to Fig. 13 the fluid is absorbed because in case of $k \neq 1$ (when there is no hydrostatic pressure) the deformation of grains is not dominant although the closed pores (inside and among the grains) are open and create a new micro-crack system with increased pore volume.

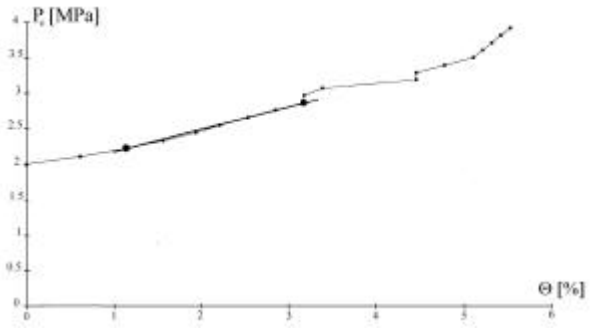

Fig. 13: Changing of the relative pore fluid volume in case of drained triaxial test (k = 20).

5. Conclusion

Four different triaxial tests were carried out during the research with saturated limestone. Two of them were under drained conditions and two of them were under undrained conditions. In undrained conditions the determine microcrack propagation from the deviatoric stress-strain curves is equal to the maximal value of the pore fluid pressure. With decreasing the lateral load under undrained conditions (k = 10 and k = 20) the maximum value of the pore water pressure is in ratio of the dilation limit of the $s_1 - e_v$ curve and this ratio is inverse to k.

Under drained conditions the grains and the bonds were linearly deformed. During the drained triaxial tests with constantly increasing stress (k = 10 and 20) the fluid was absorbed because in case of $k \neq 1$ the deformation of grains was not dominant although the closed pores were open and create a new microcrack system with increased pore volume.

Acknowledgements: The authors are indebted to Prof. F. Homand for her expert help in performing the experiments. The work has been made possible through a grant by the French Government Scholarship (BGF) and the National Scientific Research Foundation of Hungary (OTKA F022620).

References

1. Brace, W. F., 1964, *Brittle Fracture of Rocks*. In.: State of stresses in Earth's crust: Proc. Int. Conf., Santa Monica, 110-178.
2. Bieniawski, Z. T., 1967, *Mechanism of Brittle Fracture of Rock.* CSIR Report, Pretoria, South Africa.
3. Eberhardt, E., Stimson, B. & Stead, D., 1999, Effects of Grain Size on the Initiation and Propagation Thresholds of Stress-Induced Brittle Fractures. *Rock Mech. Rock Engng.* 32(2), 81-99.
4. Lajtai, E. Z. & Lajtai, V. N., 1974, The Evolution of Brittle Fracture in Rocks. *J. Geological Sci.* 130(1), 1-18.
5. Lajtai, E. Z., 1998, Microscopic Fracture Processes in a Granite. *Rock Mech. Rock Engng*. 31(4), 237-250.
6. Martin, C. D. & Chandler, N. A., 1994, The Progressive Fracture of Lac du Bonnet Granite. *Int. J. Rock Mech. Min. Sci. & Geomech. Abstr*. 31(6), 643-659.
7. Wawersik, W. R. & Fairhurst, C., 1970, A Study of Brittle Rock Fracture in Laboratory Compression Experiments. *Int. J. Rock Mech. Min. Sci. & Geomech. Abstr*. 7(5), 561-575.
8. Cook, N. G. W., 1970, An Experimental Proving that Dilatancy is a Pervasive Volumetric Property of Brittle Rocks Loaded to Failure. *Rock Mech. Rock Engng*. 2(3), 181-188.
9. Deli, Á., 1991, *Essais Triaxiaux sur un Gres et un Calcaire*. Diplom Etude d'Approfondies de Genie Civil et Miner, Laboratoire de Géomécanique, INPL, ENSG-Nancy.
10. Deli, Á. & Vásárhelyi, B., 2000, Investigation of the Fracture Process with Different Loading Paths Triaxial Tests on Saturated Sandstone. *Bull. Engng. Geol. Env*. 59(3), 184-193.
11. ISRM, 1981, *Rock Characterization Testing and Monitoring*, ISRM Suggested Methods, Edited: Brown, E. T., Pergamon Press, Oxford, 107-127.